MEASUREMENT OF BACKSCATTERING FACTOR FOR X RAY CALIBRATION BEAM WITH VARIOUS PHANTOMS USING IONIZATION CHAMBER AND THERMOLUMINESCENT DOSIMETER

ROKSHANA PARVIN NUPUR

M.Sc. ENGINEERING THESIS

DEPARTMENT OF NUCLEAR SCIENCE AND ENGINEERING
MILITARY INSTITUTE OF SCIENCE AND TECHNOLOGY
DHAKA, BANGLADESH

SEPTEMBER 2022

MEASUREMENT OF BACKSCATTERING FACTOR FOR X RAY CALIBRATION BEAM WITH VARIOUS PHANTOMS USING IONIZATION CHAMBER AND THERMOLUMINESCENT DOSIMETER

ROKSHANA PARVIN NUPUR (SN. 1015280023)

A Thesis Submitted in Partial Fulfillment of the Requirements for the Degree of Master of Science in Nuclear Science and Engineering

DEPARTMENT OF NUCLEAR SCIENCE AND ENGINEERING
MILITARY INSTITUTE OF SCIENCE AND TECHNOLOGY
DHAKA, BANGLADESH

SEPTEMBER 2022

MEASUREMENT OF BACKSCATTERING FACTOR FOR X RAY CALIBRATION BEAM WITH VARIOUS PHANTOMS USING IONIZATION CHAMBER AND THERMOLUMINESCENT DOSIMETER

DECLERATION

I hereby declare that the study reported in this thesis entitled as above is my own original work and has not been submitted before anywhere for any degree or other purposes. Further I certify that the intellectual content of this thesis is the product of my own work and that all the assistance received in preparing this thesis and sources have been acknowledged and/or cited in the reference Section.

Rokshana Parvin Nupur

Department of Nuclear Science and Engineering, MIST, Dhaka

ACKNOWLEDGEMENTS

First of all, I am grateful to the almighty Allah for giving me the courage and enthusiasm to complete the project work.

This project and the thesis paper are two of the greatest additions to my insufficient knowledge and experiences. I would like to express my deep gratitude to my research supervisor, **Dr. Md. Shakiur Rahman,** Chief Scientific Officer of secondary standard dosimetry laboratory (SSDL), Bangladesh Atomic Energy Commission (BAEC) and Director, Nuclear Safety Security and Safeguards Division (NSSSD) of Bangladesh Atomic Energy Commission (BAEC), Agargaon, Dhaka, for his patient guidance, enthusiastic encouragement, and useful critiques of this research work. I would also like to thank my co-supervisor, **Dr. Md. Azizur Rahman,** Professor, Department of Nuclear Science and Engineering, MIST, Dhaka, for his advice and assistance in keeping me updated on this project.

I'd also like to thank my Department Head, **Col. Molla Md. Zubaer, SPP, te.**, Former Department Head, **Col. Salahuddin Zafor**, our Program Coordinator. **Lt. Col. Foysal Kadir,** and Former Program Coordinator, **Lt. Col. Md. Altab Hossain PhD**., for their unwavering support and guidance from the very beginning and all through the seven-year eventful journey.

Finally, and not least, I wish to thank all of my classmates and office staff for their support and encouragement throughout the study and thesis work.

ABSTARCT

MEASUREMENT OF BACKSCATTERING FACTOR FOR X RAY CALIBRATION BEAM WITH VARIOUS PHANTOMS USING IONIZATION CHAMBER AND THERMOLUMINESCENT DOSIMETER

Radiation hazard is one of the critical issues at different medical centers, industries and nuclear facilities around the world. To protect radiation workers, public and environment, a reliable dose measurement system is required that should be complied with international recommendations. X-rays and gamma rays are a highly penetrating radiation and are widely used as a calibration source at different of medical facilities, industries and nuclear facilities. X-ray beam characterization for the calibration of radiation measuring equipment is necessary to meet the recommendations by international organizations. In the present study, characterization of X-ray beam generated from X-ray irradiator, Model: X80-225KV, Hopewell Design, Inc of Secondary Standard Dosimetry Laboratory (SSDL) has been performed in accordance with the ISO 4037-1 narrow–spectrum series. The beam characterization was done by the determination of Half-Value Layer (HVL), the Effective Energy, Homogeneity Coefficient (HC), Beam Quality Index and output air Kerma values. Experimentally measured HVL is compared with the values recommended by ISO-4037 and very small deviation is found. Filter thickness error or positioning of ionization chamber may be reason for this. The homogeneity coefficient is between 0.46 to 0.50. The homogeneity coefficient should be 1 but due to beam hardening, it is not possible. The Effective Energy, Eeff for ISO narrow spectrum series were calculated by empirical relation derived from Hubble mass attenuation coefficients. Hence, a set of conversion coefficients has been established for the effective energies of photon beam from air Kerma to dose equivalent (Sv/Gy) i.e., for ambient dose equivalent, H*(10) and personal dose equivalent, $H_P(10)$ & H_P (0.07) for ISO beam code N40, N60, N80, N100, N120, N150 and N200 by empirical mathematical relationship applicable for the photons with energies between 10 keV to 10 MeV. The measured dose H*(10), $H_P(10)$ & $H_P(0.07)$ could be used for implementation of the new ICRU operational unit in radiation monitoring around the radiation facilities to protect human and environment in Bangladesh. An evaluation of backscattering factors for ISO water phantom and ICRU slab phantom has been conducted by MCNPX Code (version 2.6.0). for tube

potential N80, N100, N120 and N140. The calculated values were compared with the values of experimental values. It is found that in personal dose monitoring, the backscattering factor contributes a considerable amount to the total absorbed dose.

TABLE OF CONTENTS

LIST OF TABLES

CHAPTER 1
INTRODUCTION

1.1 Background of the Problem

Radiation hazards are one of the most critical issues at different medical centers, industries, and nuclear facilities around the world. To protect radiation workers, the public, and the environment, a reliable dose measurement system is required that should comply with international recommendations. X-rays and gamma rays are highly penetrating radiation and are widely used as calibration sources at different medical facilities, industries, and nuclear facilities. Absorbed dose quantification of the extent of air kerma in the human body is a great challenge to optimize radiation protection. Human-body-related protection quantities are not measurable in practice; therefore, they cannot be used directly as quantities in radiation monitoring. Over the years, the International Commission on Radiation Units and Measurements (ICRU) has developed definitions of operational quantities in radiation protection and has published corresponding values of conversion coefficients (Sv/Gy) from fluence to the operational quantities for mono-energetic photons and particles of several types (photons, electrons, neutrons, and others), as well as conversion coefficients from total air kerma to dose equivalent. The dose-equivalent quantities are produced by the corresponding expanded and aligned field in the sphere of the International Commission on Radiation Units and Measurements (ICRU) at a depth of 10 mm on the radius opposing the direction of the field. The ICRU sphere is 30 cm in diameter, and its density equals 1 g/cm^3. This sphere consists of 4-elemental compositions of 76.2% oxygen (O), 11.1% carbon (C), 10.1% hydrogen (H), and 2.6% nitrogen (N). Most of the national recommendations for the calibration of dosimeters are derived from the recommendations of ISO 4037; they specify the characteristics of calibration beams. To reproduce these beams strictly according to the ISO recommendation is difficult and requires a close compromise. The ISO 4037 also describes procedures for calibrating and determining the response dose rate meters and personnel dosimeters in terms of the ICRU operational quantities H*(10), H′(0.07), and Hp (10), Hp (0.07) for radiation protection. Analyzing the beam quality of an X-ray irradiator is done by calculating several parameters, such as the half-value layer, effective energy, homogeneity coefficient, and beam quality index. These values will be compared with ISO values**.** A set of conversion coefficients from the air kerma to H*(10), H′(0.07), and Hp (10), Hp (0.07) is required to protect radiation

workers and patients from radiography exposure and to reduce the stochastic effect of radiation (cancer and hereditary effects).

The backscattering factor (BSF) is the difference between the collision kerma of a material at the surface of a full scatter phantom at a position in the beam axis and the collision kerma of the same material at the same place in the primary beam when there is no phantom present. Experimental measurement of backscatter factors is challenging, and tabular values are frequently based on Monte Carlo calculations. In this study, we used the Monte Carlo N-Particle (MCNP) Code (version 2.6.0) to compute the backscattering factor. The experimental values are contrasted with these values.

1.2 Motivation of the Study

In the past, inadequate calibration facilities have caused large errors in some dose estimations received by the radiation workers and population. This is especially true in developing countries like Bangladesh, where limitations exist for adequate funding and expertise.

In order to ensure radiation protection, different types of radiation measuring equipment, such as survey meters, pocket dosimeters, contamination monitors, and personal dosimeters, are usually used in the radiation field. The problem associated with the use of radiation measuring instruments has recently been the subject of much international interest because overexposure can produce undesirable biological damage to exposed persons. A little can also be done to alleviate the suffering of the exposed person.

Due to this fact, radiation measuring instruments or devices should be calibrated properly for radiation workers, the public, and the environment as per international recommendations.

1.3 Significance of the Study

Ionizing radiation is a factor with indispensable benefits, but with its reckless use and irrational exposures, it can lead to serious health problems. X-rays involve ionizing radiation that can deposit energy in human cells and cause tissue changes. It is important to minimize any associated risk to the patient. This is done by limiting the radiation exposure to the minimum required to create the clinical images needed to answer the medical question.

Based on the ICRP recommendations, the negative biological effects of ionizing radiation exposure can be divided into two general categories. The first one contains the biological effects caused by the exposition to high doses, so-called deterministic effects. These follow immediately after the exposition, when a certain threshold of dose is crossed. The second category contains the biological effects that are caused by low doses of ionizing radiation, so-called stochastic effects. For stochastic effects, there is no threshold level at which biological effects do not occur. These effects do not cause immediate clinical manifestations, and they are unpredictable. They mainly damage the cell itself, and the biological effects can be seen after several years go by.

It is necessary to emphasize the safe and effective use of ionizing radiation. To be able to prevent unwanted biological effects of radiation in the human body, epidemiology studies, regular education of the medical workers, and informing them about the effects and mechanisms of this radiation on human cells are necessary. Hereby, it is inevitable to know the sources of the ionizing radiation and the ways to lower the exposure to the lowest possible level while keeping the maximum benefit.

1.4 Research questions

In Bangladesh, ionizing radiation is widely used. Various types of radiation monitoring devices, such as ion chambers, survey meters, etc., are being used to properly measure different radiation dose levels, mainly in hospitals, clinics, and research facilities. To ensure the safety of the public, environment, and workers from radiation hazards and get maximum benefit from ionizing radiation, the instruments should be calibrated appropriately. Every radiation facility should have at least one calibrated radiation measuring instrument. Calibration ensures that radiation protection measuring instruments are working properly for future purposes.

The application of ionizing radiation in medicine, industry, and research institutes in Bangladesh has not yet reached the same level relative to its population as in other industrialized countries. In order to achieve the maximum benefit from the use of such radiation, it is essential that dosimeters be calibrated with respect to the correct dose or dose rate indication. How can we minimize X-ray radiation exposure? Are radiation monitoring devices available in our country? Is ionizing radiation good for the human body? Which devices are commonly used for radiation monitoring?

1.5 Objectives of the Study

The main objectives of the present study are:

- Characterization of an X-ray beam irradiator.
- A set of conversion coefficients for personal dose equivalents, $H_P(10)$ and $H_P(0.07)$, and ambient dose equivalents, H*(10), were derived from an empirical mathematical relationship applicable for monoenergetic photons with energies between 10 KeV and 10 MeV. These conversion coefficients were eventually used to measure ambient dose equivalents and personal dose equivalents.
- Measurement of backscatter (BSF) factors for various phantoms.
- Simulation of the backscatter (BSF) factor using the MCNP code.

An X-ray machine has been installed at SSDL, AERE, Savar, Dhaka for the purpose of calibrating radiation measuring instruments according to user beam qualities. In this type of X-ray machine, the tube voltage, tube current, and stability parameters are known and specific to each beam quality. The filter thickness and composition of material are followed according to the ISO 4037 standard. Before using an installed X-ray machine, it is essential to verify the beam quality of an X-ray irradiator, like the half-value layer, homogeneity coefficient, and effective energy, with the ISO values.

1.6 Outline of the Thesis

Chapter 2: Theoretical Study: discusses radiation and its pros and cons.

Chapter 3: Literature Review: In this section, some literature reviews related to my thesis are mentioned and written as a summary.

Chapter 4: Methodology: This chapter briefly explains the methodology that has been followed for this thesis.

Chapter 5: Results and Discussion: Based on the experiment, experimental results and simulation results were shown in some tables and grapes.

Chapter 6: Conclusion and Recommendations: In this section, the results were expounded, and experimental results were compared with national and international values.

CHAPTER 2
THEORITICAL STUDY

2.1 Radiation

Radiation is the secretion or transmission of energy in the form of waves or particles through space or through a material medium, such as those that characterize light rays and X-rays.

Radiation is broadly classified into two groups:

- Ionizing radiation
- Non-ionizing radiation

Radiation with adequately high energy can ionize atoms; that is to say, it can knock electrons out of atoms and create ions, just as lower-energy radiation can break the chemical bonds within molecules.

Ionizing radiation is radiation that has enough energy to remove tightly bound electrons from an atom's orbit during an encounter with the atom, causing the atom to become charged or ionized. Ionizing radiation creates a health concern by destroying tissue and DNA in genes because it has the ability to alter the atoms in living things. X-ray devices, cosmic rays from space, and radioactive materials all emit ionizing radiation.

Non-ionizing radiation has sufficient energy to shift atoms in a molecule around or cause them to vibrate, but not adequate energy to remove electrons from atoms. Examples of this kind of radiation are radio waves, visible light, and microwaves.

2.2 Interaction of gamma rays

Even though there are a large number of potential interaction processes for gamma rays in matter, just three key types—the photoelectric effect, Compton scattering, and pair production—are crucial for radiation measurements. All of these processes result in the conversion of gamma-ray or photon energy to electron energy, either partially or fully. They cause abrupt and unexpected changes in gamma-ray energy because the photon either entirely vanishes or is scattered at a sizable angle.

Photoelectric effect

The low-energy photon connects with a bonded electron inside one of the atom's many shells during the photoelectric absorption process, transferring all of its energy to the electron, which is subsequently released from the atom as a photoelectron.

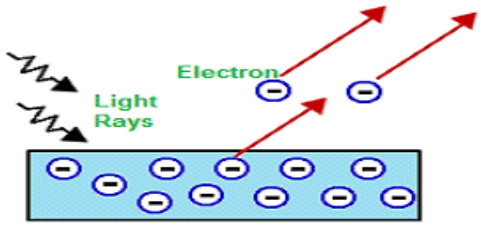

Fig. 2.1: Photoelectric effect

Compton Scattering

The incident photon collides elastically with an electron that is free or only loosely bound, imparting momentum and energy to the electron. The electron is subsequently accelerated, and the photon is deflected with less energy.

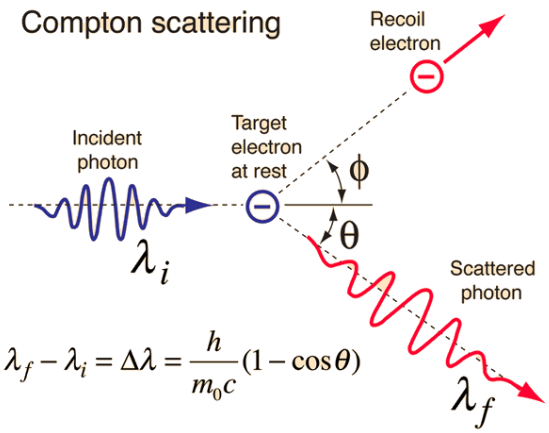

Fig. 2.2: Compton Scattering

Pair Production

The arrangement of two electrons, one of which is negative and the other positive, or positron, is known as pair creation. A continuous transformation of radiant energy into matter is called pair creation. It is a significant mechanism by which high-energy gamma rays are taken up by matter. The electromagnetic energy must be at least equal to the mass of two electrons for pair formation to take place.

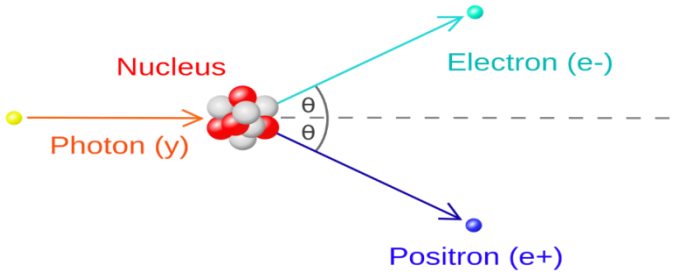

Fig. 2.3: Pair Production

2.3 X-rays

Due to their usage in medicine, almost everyone has heard about X-rays. While X-ray and gamma rays come from various regions of the atom, they share the same essential characteristics. X-rays are released from the nucleus' exterior.

The German physicist Wilhelm Roentgen discovered X-rays in 1895, and he gave them their unusual name because of this. These rays, which were invisible, unlike regular light, and traveled in straight lines, had the same effects on photographic film as light. However, they were more piercing than light, and they had no trouble piercing the human body, wood, fairly thick metal, and other "opaque" things.

2.3.1 Production of X-rays

When electrons collide with a metal object, their speed suddenly decreases, producing X-rays that are commonly referred to as "braking radiation" or bremsstrahlung. If the bombarding electrons are powerful enough, they may be able to knock an electron out of the target metal atoms' inner shells.

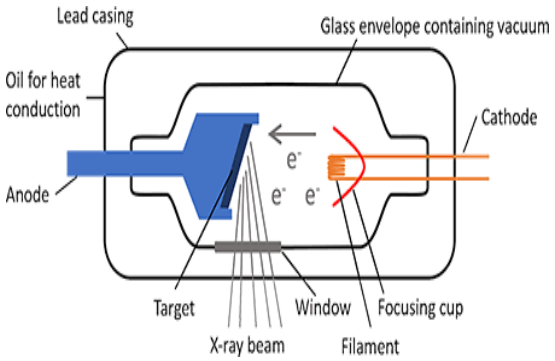

Fig. 2.4: A simple X-ray production unit

2.3.2 Types of X-rays

The accelerated electrons' interactions with the electrons of tungsten nuclei inside the tube anode result in the production of X-rays. Bremsstrahlung radiation and characteristic radiation are the two different forms of X-rays that are produced.

- **Characteristic radiation**

A "hole" is left in the inner layer of the tungsten atom when a high-energy electron collides with an inner shell electron. An outer shell electron that is generating X-rays due to energy loss fills this space.

- **Bremsstrahlung/Braking X-ray Radiation**

An electron gets slowed down and has its course altered when it moves close to the nucleus. Bremsstrahlung X-ray photons are released when energy is lost.

Bremsstrahlung = Braking radiation

2.4 **Effects of radiation**

The radioactive disintegration of atomic nuclei produces penetrating electromagnetic radiation known as gamma rays, or gamma radiation. Its electromagnetic waves have the shortest wavelengths.

The amount of radiation exposure damages the health. Two broad categories of health consequences exist. Both stochastic and non-stochastic effects are present.

2.4.1 Stochastic effects

Stochastic effects are those that happen when someone receives a high radiation exposure. Years after exposure, stochastic effects frequently become evident. Stochastic effects, on the other hand, lack a threshold dose. It is impossible to determine with certainty that a case of cancer or genetic damage was caused by exposure to radiation since stochastic effects can occur in people who have not been exposed to radiation above background levels. Two categories of stochastic effects exist. They are genetic and somatic stochastic effects, respectively.

2.4.2 Non-stochastic effects

Non-stochastic effects, in contrast to stochastic effects, have a threshold dose below which they do not manifest. In other words, there is a connection between the exposure and the effect in non-stochastic effects. Additionally, the size of the dose directly correlates with the strength of the impact. When extremely high radiation doses are obtained within a short period of time, non-stochastic effects frequently follow. These effects frequently become obvious within a few hours or days. Skin and tissue burns, cataract formation, sterility, radiation illness, and death are a few examples of non-stochastic consequences. Each of these consequences is unique from the others, and each can result in sickness or death, depending on the threshold dose and the length of time the dose was administered.

2.5 Backscattering Factor (BSF)

The backscatter factor is important for measuring the absorbed dose. A backscatter factor is defined as a ratio of the kerma rate to water at the surface of the water phantom to the kerma rate to water at the same point in space in the absence of the phantom. The backscatter factor depends on the X-ray field size, the X-ray spectrum, and the thickness and composition of the patient or phantom. The evaluation of the backscattering factor based on water phantom materials was conducted by the MCNPX Code (Version 2.6.0). The formula for the backscattering factor is given below:

$$\text{Back Scattering Factor (BSF)} = \frac{\text{The absorbed dose in the surface layer of a phantom}}{\text{Theabsorbeddoseinthesamematerialintheabsanceofscatteringmaterial}}$$

The importance of the BSF in determining the absorbed dose at the surface of a patient is clear, but achieving an accurate measurement of this factor is not simple. The BSF measurement is confounded by several factors, depending on the type of detector that is used. For ionization

chambers, there are competing effects: the displaced material in the chamber volume results in a lack of scatter being created within the chamber, and also more scatter occurring posterior to the chamber due to a lack of attenuation.

2.6 Purposes of Calibration

The calibration process has three main goals. Here are several examples:

- To verify that a device is functional and, hence, capable of serving the monitoring needs for which it was designed.
- To calculate the reading of an instrument as a function of the value of the measured quantity (the quantity meant to be measured), under a regulated set of standard conditions. This needs to be done across the instrument's whole range of readings.
- If at all possible, the instrument's overall measurement accuracy is optimized in order to alter the calibration.

2.7 Principles for Radiation Protection

The main goal of radiological protection is to offer an adequate level of protection against ionizing radiation for people. The crucial framework for achieving this goal is to maintain doses below the pertinent thresholds in order to prevent the appearance of deterministic effects, as well as to make sure that all practical precautions are taken to delay the onset of stochastic effects. The following basic concepts serve as the foundation for the radiological protection system for proposed and ongoing practices:

- The justification of practice:

In theory, radiation exposures must be justified with the consent of relevant professional associations.

- The optimization of protection:

The magnitude of individual doses, the number of people exposed, and the likelihood of exposures where these are not certain to be received should all be kept as low as reasonably achievable (ALARA) for any given source within a practice, taking economic and social considerations into account.

- Individual dose and risk limits:

The dose given to individuals must not go over the ICRP-recommended upper limits in the appropriate situations. These are designed to guarantee that no person is ever exposed to

radiation risks that are deemed unacceptable by these methods. The main goal of dosage limitation is to impede non-stochastic effects and limit the occurrence of stochastic effects to a manageable level.

CHAPTER 3
LITERATURE REVIEW

In this study, an X-ray irradiator is used to establish and analyze the beam quality of the X-ray. There is some literature related to the analysis of beam quality and measurement of back scatter factor using different techniques worldwide. Some literature studies most relevant to this research work are mentioned below with proper information.

Dosimetry characterization of calibration X-ray beams for radiation protection and measurement has become an important topic in the research field of medical physics in Bangladesh. While reviewing past works on the response of gamma radiation and X-ray radiation, they are quite diverse in nature. A brief review of these works is presented below:

A calibration procedure has been developed by W.W. Moschler Jr. and E.F. Dougal for a direct scanning densitometer that is used for analyzing the quality of wood by two gamma radiation sources (Am-241 and Fe-55). The linear attenuation coefficient and mass attenuation coefficient have also been measured, and these values are compared with the values of different handbooks. Little error is found due to the presence of moisture, imperfect collimation, and the presence of extractives.

Marc Desrosiers et al. describe the importance of dosimetry in radiobiology, like the effect of radiation dose. When researchers deal with radiation doses, they must be aware of both accuracy and precision. The factors, i.e., filter property, buildup factor, distance, and depth dose, all govern the radiation dose and its distribution. The journal also describes the role of primary and secondary dosimetry labs, the current status of radiobiology dosimetry, etc.

J. W. Hopmans and J. H. Dane determined the calibration constant for the soil sample at different points by using a dual-energy gamma source and calculating soil properties. They used two gamma energy sources, Am-241 and Cs-137, and measured the count per second using Beer's law. They were able to calculate the calibration constant for each source at different positions in the soil sample.

The operational experience gained by Clarke et al. in the dosimeter calibration facility at the Berkeley Nuclear Laboratories of the Central Electricity Generating Board showed that the keytools, a 400 keV positive ion accelerator and a 250 keV X-ray set, had proved sufficient for the accurate calibration of health physics dosimeters. The sealed sources employed at the

facility were acceptable for routine calibration purposes but could be more closely correlated to the national standards used for bremsstrahlung radiation.

M.S. Rahman has studied the response of GM tubes and ionization chamber-type survey meters to different gamma-ray photons. The ionization chamber type survey meter shows better linearity than the GM tube type survey meter for the energy range of 36 KeV to 662 KeV.

Khalid R.O. has studied the calibration of a radiation survey meter using a Cs-137 gamma source at the Secondary Standard Dosimetry Laboratory of Sudan. The survey meter RADOS was also considered suitable for measurements according to the results obtained for its uncertainties. The measurements indicated the importance of having the orientation of the instrument at the sensitive point at an angle of 0° (i.e., in the direction of the beam of radiation to be measured).

Sumaiya has studied the dosimetry of the gamma field in characterizing radiation measuring instruments in Bangladesh at some different distances for different radiation qualities and air kerma rates at various distances. A linearity test and an angular response have been calculated. She also establishes a set of conversion coefficients for kerma to H*(10).

Masud has verified the ISO standard radiation beam quality based on the determination of the ambient dose rate H*(10) and subsidiary chamber calibration factor. The dosimetric comparison of the three protection levels in the ionization chamber has also been illustrated by measuring the ambient dose rate of the Co-60 source. The minimum and maximum percentages of relative intrinsic errors between chambers are found to be 3.27 and -6.02.

The calibration of a portable gamma-ray spectrometer was achieved by Gibson and Burt with standard sources and a multichannel analyzer. The results were compared with data from other workers. Reasonable agreement was demonstrated. The conversion of peak height to photo flux or dose was obtained from a series of graphs obtained by calibration or, less accurately, from a monogram. The spectrometer was used for surveying around nuclear installations.

The calculation of the angle dependence of response and also the energy response of the simplified design of the photon personal dosimeter and its relationship with the recommended ICRU calibration quantity was carried out by Bartllet et al. The results of calculations for a simplified design of a personal dosimeter to measure H_P (10) for photon radiation were discussed. The design consists of a tissue-equivalent detector in the form of a 1mm-thick disc of radius 2.5 or 5mm covered with a hemisphere of tissue-equivalent material of 1cm radius.

T. Siddiqua, M.S. Shakilur has studied about the X-ray calibrator, which is profound with the standard procedure recommended by ISO 4037 in terms of ambient dose and personal dose equivalent. Characteristics such as half-value layer, homogeneity coefficient, effective energy, and conversion coefficient have been studied.

Chan and Doi investigated the backscattering factor for mammography units with a Mo-anode (0.03 mm additional Mo-filter) and a W-anode (1 mm added AI filter) using Monte Carlo methods. They have employed a geometry that causes all photons to strike the phantom perpendicularly at the same location (a pencil beam), registering all energy impartations along the way, creating a lateral, endless phantom. Their method is analogous to calculating depth doses in a phantom exposed to a wide beam of photons that are incident perpendicularly. The depth dosages were forced to zero depth in order to receive the backscatter factor. Water, fat, 50% water + 50% fat, and Lucite are the four phantom materials for which back scattering factors have been reported.

Chan and Doi have also reported an interesting simulation of how a LiF-dosemeter measures the backscattering factor. They have calculated the average absorbed dose in the dosemeter with and without the phantom present. The resulting back scattering factor is significantly lower than that calculated without a dosemeter (up to 7% with a water phantom). Their calculations of the average absorbed dose are not presented in detail. It is somewhat astonishing that, in their calculations, the use of a phantom equivalent dosemeter of the same dimensions as the LiF-dosemeter results in approximately the same (only slightly smaller) underestimate of the BSF, even if LiF has a 2.5 to 3.5 times higher density than the different phantom materials.

CHAPTER 4
METHODOLOGY

4.1 Overview

In 1991, the Secondary Standard Dosimetry Laboratory (SSDL) was installed at the Bangladesh Atomic Energy Commission. The Bangladesh Atomic Energy Commission is situated in Savar. The laboratory has been established to offer calibration services and dosimetric measurements with the maximum degree of accuracy.

This chapter describes various pieces of equipment that were used in this research. To complete this research, the SSDL laboratory and different equipment from this laboratory are used. We used the X-ray 225kV beam irradiation systems, a 600cc secondary ionization chamber (NE 2575#0386, dose-1 electrometer, thermometer, barometer, different filters, phantoms, thermoluminescent dosimeter (TLD), etc. Their working principles and specifications are described below this section.

4.2 MODEL X80-225KV X-ray Beam Irradiator

For the effective utilization of peculiar radiation properties, X-rays are widely used in various nuclear plants. In order to evaluate the radiation dosimeter response utilized for the protection of radiation as a whole, it is crucial to characterize the x-ray field for use in calibrating standardization. The calibration x-ray unit's specifications are listed below:

Model: X80-225KV X-ray Beam Irradiator:

Type: X80-225KV

Serial No.: 1922-1205

Tube Potential: 15-225kV in 0.2kV increments

Tube Current: Current selectable from 0-50 in 0.05mA increments.

Cooler: Water.

Fig. 4.1: X80-225kV X-ray Beam Irradiator

The main sub-systems of the X-ray system are

1. the dosimetry-grade X-ray system
2. the shielded enclosure
3. the beam shutter and collimator
4. the filter assembly
5. the system control panel and status indicators
6. all control and signal cables

Dosimetry-Grade X-ray System

The comet tube head, generator, and controller are components of the dosimetry-grade X-ray system. Together with the other subsystems, the X-ray set is integrated. The following components make up the X-ray system:

1. Tube head
2. Controller
3. High voltage generator
4. Electrical power supply
5. Water cooler
6. All necessary cables for operation

4.2.1 Beam Shutter and Collimator

Inside the shielded container, fastened to the face of the door, is a high-speed shutter. A collimator that opens the tungsten shutter, an electric solenoid, and a pivot mechanism make up this device.

The tube head's beam port has a tungsten collimator attached to regulate the beam's size. The shield's collimated port and this opening work together to create a beam with a 25-degree solid angle.

A tungsten disk of 32 mm in diameter and 15 mm thick makes up the shutter. It conceals the beam port when shut. A spring pushes the shutter shut when the solenoid's electricity is switched off. Electric switches provide an indication of the shutter's open or closed positions.

4.2.2 Filter assembly

The filter assembly is designed to alter the X-ray beam's special characteristics in order to satisfy various beam codes required for equipment calibration. It consists of a 38-centimeter metal disk that is mounted on the front of the shielded container. The disk is rotated at 3 rpm by a motor and pulley. Approximating sensors detect the selected filter when it is in position and turn off the motor. Positioning accuracy is 0.5 mm or less. Sequential numbers (1–10) and the beam code are written on the disk. The pores on the disk are designed to fit filters with thicknesses ranging from 0.1 mm to 15 mm. The disk may easily be taken out and another disk added when there are more than 10 users. The ISO 4037-3,1999 "X and Y reference radiations for calibrating dosimeters and dose rate meters and for determining their response as a function of photon energy" calls for a set of filters to construct the beam definitions. The filters are made of high-purity copper, aluminum, and other materials as needed to achieve the aforementioned beam specifications. The following filters are included with the filter wheel

Table 4.1: Filter Wheel #1: ISO 4037 Beam Qualities

	Quality No	H.V (kV)	Al (mm)	Cu (mm)	Sn (mm)	Pb (mm)
1	N40	40		.21		
2	N60	60		.60		
3	N80	80		2.00		
4	N100	100		2.50		
5	N120	120		5.00	1.00	
6	N150	150			2.50	
7	N200	200		2.00	3.00	1.00
8	N250	250			2.00	3.00

4.3 NE-2575 reference standard ionization chamber with volume 600 cc Detector Chamber

Features

- vented sensitive volume of 600 cc
- Suitable as high precision reference chamber for radiation protection dosimetry
- Suitable for survey meter calibration
- Superior energy response, directional dependence and long-term stability

It has very little variations of response with radiation quality from low X-ray energies up to high energy photon radiation.

Fig. 4.2: NE2575#386 (600cc) cylindrical ionization chamber

4.4 Electrometer

An electrometer is a device that is used to measure the electric charge or electrical potential difference. There are various types of electrometers; here we use the Dose1 electrometer. The dose 1 is a portable, single-channel, reference-class dosimeter according to IEC 60731 for dosimetry using ionization chambers and semiconductor detectors. Due to the high dynamic range of the measuring channel, a very basic range selection depending on the type of detector connected is sufficient for most applications.

The wide range of power supplies allows worldwide use without operator intervention. In addition, there is the possibility of using instruments with accumulators and with alkali manganese batteries of low impedance. The polarization voltage is produced by a DC/AC converter from a 5 V internal supply voltage. The polarity and value can be programmed in the range of +/- 600 V. In the event of a fault, the active current limitation keeps the short-circuit current safety below 0.1 mA.

When an instrument is equipped with the convertible option, practically all types of radiation detectors can be connected using sensors; radioactive detectors can be connected using sensor-specific adapter cables. This allows automatic switching between floated and grounded input technology. Dose 1 software runs under Windows XP, Service Pack 2, and Windows 2000, Service Pack 4. This program is used to define and modify sensors, radioactive check sources, and application-specific correction factors. The communication between the dosimeter and the PC is maintained via an RS-232 serial interface.

Dose1 software is available in two versions: Standard and Admin. A complementary program, Dose1 measurement, can be installed with the admin version. Dose1 measurement provides functions for measurement setup, start/stop measurement, and saving of data.

Table 4.2: Specification of Electrometer

Item	Value
Stem Material	Stainless steel
Enclosure Material	ABS plastic and epoxy
Effective measurement point in mm	0.8±0.2 from surface
Chip size in mm	0.95X0.95X0.4
Active detector diameter in mm	0.6
Active detector thickness in mm	0.02
Head diameter in mm	4
Head length in mm	15
Sterm diameter in mm	4
Total length in mm	60
Cable lenth in m	2
Cable	Low noise coaxial
Connector	Triaxial, TNC or BNC
Sensitivity in nC/Gy	4.1
Leakage current in Pa	≤ 2
Typical Dose linearity in %	< 0.2
Energy dependence in %	±0.5
Temperature dependence in %/Celsius	0.05

Fig. 4.3: Dose 1 Electrometer

4.5 Barometer

A barometer is an instrument that measures the atmospheric pressure. In this study, it is used to measure the pressure in the experimental room.

Some features of a Barometer

1. *Measuring ranges:* 920 . . .1050 hPa
2. *Accuracy:* ± 1 hPbei 20^0C ($\pm 1^0$C)
3. *Resolution and scaling:* ≤ 0.5 hPa/0.5 hPa
4. Temperature compensated work
5. Small, compact, practical
6. Without battery
7. With memory pointer

Fig. 4.4: Barometer

4.6 Thermometer

A thermometer is a temperature-measuring instrument. In this study, a digital precision pocket thermometer (GTH 175/PT) was used for measuring the temperature of the room.

Fig. 4.5: A digital pocket thermometer.

4.7 Thermoluminescent Dosimeter (TLD)

A thermoluminescent dosimeter, or **TLD,** consists of a piece of thermoluminescent crystalline material inside a radiolucent package. It is used to calculate the dose of ionizing radiation. In this study, we have used a thermoluminescent dosimeter to measure the absorbed dose of X-ray radiation. Some common features of Radpro TLD are given below:

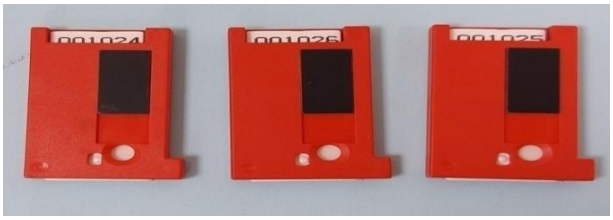

Fig. 4.6: RadPro TLD

Table 4.3: Specification of RadPro TLD

	MTS (LiF:Mg,Ti)	MCP (LiF:Mg,Cu,P)
Radiation:	Beta, gamma, X-Rays, neutron (except 7LiF)	Beta, gamma, X-Rays, neutron (except 7LiF)
Measurement range	50μGy – 10Gy	10μGy – 10Gy
Main TL peaks:	210°C	210°C
Efficient atomic no.:	8.2	8.2
Linearity:	2% up to 2Gy	<5% up to 10Gy
Fading (22°C):	>3% in 3 month	>3% in 3 month
Annealing:	400°C 1h + 100°C 2h	240°C 10min
Relative sensitivity to TLD-100:	1	>15
TL emission spectrum [nm]:	400	385
Reusability:	Unlimited	Unlimited
Dose rate influence:	Independent	Independent

4.8 Phantom

Phantom is a model of the human body used to measure the effect of radiation on human beings. Water phantom is mainly used for dose measurements, because it is human soft tissue

equivalent and is universally available. In this study, we have used two phantoms. They are water phantoms and ICRU slab phantoms.

4.9 Monte Carlo Simulation

MCNP (Monte Carlo particle) is an USA-based Monte Carlo code. It is used for analyzing the transport of radiation particles, like photons, electrons, and neutrons, etc. For the simulation of a given problem using MCNP, an input file is created by declaring the necessary dimensions and source particles. After that, this file is executed using the run mode of Visual Editor Windows for MCNP code. The Monte Carlo methods are mathematical algorithms that perform numerical simulations of problems using essentially a sequence of random numbers. The MCNP method is the most accurate and effective method for dose calculations. It is because all possible physical interactions are taken into account that occurred during the radiation particle transport in the region of interest (ROI).

4.10 MCNP Input File Structure

In MCNP Monte Carlo code, the input file structure of a given problem is specified by three blocks. These are called cell cards (block 1), surface cards (block 2), and data cards (block 3). Here, the term ‘card’ is interpreted as a line of the input file. The complete problem geometry is declared with the combination of surface and cell cards. The cell cards contain material, which is specified by the material card in block 3. In fact, everything except problem geometry, such as physical interaction (using a physics card), source particle (a source card), and type of results, i.e. physical quantities (a tally card) etc., are specified by the data card.

4.10.1 Geometry Specifications

The problem geometry is primarily specified in terms of regions bounded by the first and second surfaces. The region or volume specified in this way is also called a cell. In spite of the cell card in block 1, it is convenient to discuss surface cards (block 2) first, because cells are formed by the various surface types.

4.10.2 Block 2 [Surface Cards]

Mathematically, any surface is represented by f (x, y, z) = 0. If any point at which f (x, y, z) > 0 is located in the positive sense (+) to the surface, and any point at which f (x, y, z) < 0 is located in the negative sense (-) to the surface. The layout of the surface card is,

Syntax: j a list

Where j = surface number: $1 \leq j \leq 99999$ (arbitrarily chosen by developer)

a = surface type or mnemonic

list = surface parameter

There are several surface types that can be used in MCNP, depending on the problem geometry. In this research work, we used five surface types, namely: general sphere (S), right circular cylinder (RCC), orthogonal box (BOX), truncated right-angle cone (TRC), and rectangular parallelepiped (RPP).

The right circular cylinder (RCC) is defined by a vector $\vec{V}$ (V_x, V_y, V_z) that represents the Center of the base, a vector $\vec{H}$ (H_x, H_y, H_z) that defines the axis and height of the cylinder, and the radius R.

The format is:

RCC $V_x V_y V_z H_x H_y H_z$ *R*

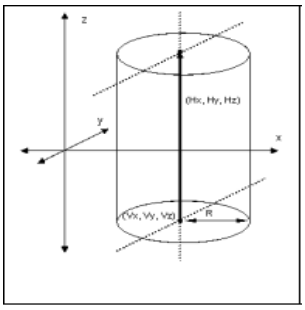

Fig. 4.7: Right circular cylinder

The suffixes are: 2.1 cylindrical surface,

2.2/2.3 plane normal to the end/ beginning of $\vec{H}$.

The orthogonal box (BOX) is specified by four vectors: $\vec{V}$ defining a corner of the box and three orthogonal vectors $\overrightarrow{A_1}$,$\overrightarrow{A_2}$, and $\overrightarrow{A_3}$ defining the three sides from the specified corner.

The syntax is

BOX $V_xV_yV_z$ A_{1x} A_{1y} A_{1z} A_{2x} A_{2y} A_{2z} A_{3x} A_{3y} A_3

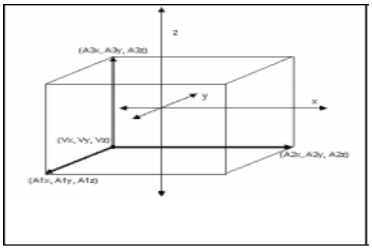

Fig. 4.8: Orthogonal Box.

The suffixes are: 3.1/3.2 planes normal to the end/beginning of A_1,

3.3/3.4 planes normal to the end/beginning of A_2,

3.5/3.6 planes normal to the end/beginning of A_3.

The truncated right-angle cone (TRC) is specified by a vector $\vec{V}$ that represents the base of TRC; a vector $\vec{H}$ represents the direction and height of the TRC axis; and R_1, R_2 represent the radius of the base and the plane perpendicular to the end of the vector $\vec{H}$, respectively.

The syntax is

TRC $V_xV_yV_zH_xH_y$ H_z R_1 R_2

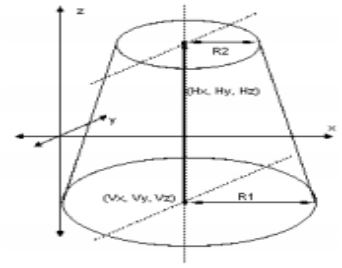

Fig. 4.9: Truncated right angle cone

4.10.3 Block 1 [Cell Cards]

A cell is formed by single or multiple surfaces and contains materials, depending on the problem geometry. The format of a cell card is as follows:

j m d geom params

Where j= cell number; $1 \leq j \leq$ 99999

m = material number, arbitrarily assigned by the developer. The material is specified on the material card for the block. It will be zero if the cell is void.

d = cell material density. A negative entry means mass density in units of g/cm^3, and a positive entry expresses atom density in units of 10^{24} atoms/cm^3.

geom = parameters, which specify the geometry of the cell using signed surface numbers and necessary Boolean operators.

4.10.4 Block 3 [Data Specifications]

Besides problem geometry, materials in cell cards, radiation source particles, the physics of particle interaction, the expected physical quantity from MCNP, etc. are specified in this specification. A brief explanation of these cards based on the developed input file is given below.

4.10 5 Materials Cards

Both the isotopic composition and the cross section library are declared using this card. The syntax of this card is,

Mm $ZAID_1$ $fraction_1$ $ZAID_2$ $fraction_2$

Where m = material number (arbitrarily specified by the developer)

$ZAID_1$ = Nuclide identification number. The full form is ZZZAAA.abX, where ZZZ is the atomic number, AAA is the mass number of the element, ab is the cross section library identifier and X is the type of data library.

$fraction_i$ = fraction of the i^{th} constituent of the material.

If fraction> 0, it represents atomic fraction and if fraction < 0 then it express mass fraction. The total mass fraction must be unity.

4.10.6 Source Specification Cards

The radiation source particle is specified by this card. The general source command ‘SDEF’ is used for defining the source particle. Besides, there are three other source commands that are also used in several problems. The format of SDEF is

SDEF parameter = value (S)

However, the value of various parameters on an SDEF card can be expressed in three different modes. They are

1 Explicitly (e.g. ERG=1.0);

2 With a distribution number (e.g. ERG=d5);

3 As a function of another variable (e.g. ERG=Fpos).

In our case, we used the first method. An SDEF card has many variables, among them those are used in this work are tabulated below.

Table 4.4: Source variables for the SDEF command

Variable	Meaning	Default
PAR	Type of particle source emits	=1 (neutron, neutron photon, neutron photon electron); =2 (photon, photon electron); =3 (electron).
ERG	Energy (MeV)	14 MeV
SUR	Surface	0 (means cell source)
VEC	Reference vector	Volume case: required unless isotropic. Surface case: vector normal to the surface with sign determined by NRM (sign of the surface normal)
DIR	μ, the cosine of the angle between VEC and the trajectory of source particle.	Volume case: μ is sampled uniformly in [-1,1] (isotropic) Surface case: p(μ) = 2μ for [0,1] (cosine distribution)
POS	Reference point for positioning sampling	0, 0, 0

RAD	Radial distance of the position from POS, in particular case it represents radius.	0

4.10.7 Physics Cards

The physics card is used to control the various physical interactions of the source particle with the material medium. As the nature of interaction varies with the radiation particle, the format of the physics card is also different for different source particles. The syntax of the physics card for photon is as follows:

PHYS: P EMCPF IDES NOCOH PNINT NODOP

The EMCPF parameter indicates the upper limit of electron energy in MeV. IDES = 0/1 indicates that Bremsstrahlung is included /is ignored for MODE P. NOCOH = 0/1 indicates that coherent scattering is included or ignored. PNINT = -1/0/1 specifies that photonuclear interactions are used in an analog manner, not used/ used with a bias. NODOP = 0/1 indicates Doppler broadening on/off. In my study, the physical interaction of photon particle is given below.

PHYS: P 100 0 0 0 1 0

Upper limit of energy 100 MeV. Bremsstrahlung production and coherent scattering are included but no photonuclear, no Doppler, no delayed gamma.

4.10.8 Tally Specifications Cards

The tally cards are used to calculated the various physical quantities, like, particle current across a surface, flux at a point, energy deposition in a cell, dose rate, etc. However, one can modify various tally cards using a tally modification card to determine the desired physical parameters. There are a total seven standard tally types available in MCNP. In this research work, we used the F1 tally, the F4 tally, and the F6 tally card.

The F1 tally card represents surface current.

The F4 tally card represents the average flux in a cell.

The F6 tally card represents energy deposition in a cell.

This tally card was also modified using tally modification card FM4 for the determination of our desired quantity-absorbed dose rate.

4.10.9 The FM card is used to convert the units of standard tally types. The FMn card modifies the cell flux of the form $\int \varphi(E)dE$ into another physical quantity, C$\int \Phi(E)dE$. The absorbed dose of water is calculated by using this car

CHAPTER 5
RESULTS AND DISCUSSION

5.1 Characterization of calibration X-ray

Radiation that penetrates deeply is an X-ray. It is also created in an X-ray tube, a highly evacuated glass tube with essentially two electrodes: a cathode and an anode made of platinum. Streams of electrons (cathode rays) are accelerated from the cathode to the anode and form X rays when they impact the anode when a high voltage is introduced between the electrodes.

Around the world, several different kinds of nuclear plants employ X-rays as a calibration source. In order to evaluate the radiation dosimeter response used for radiation protection on a whole, it is crucial to characterize the X-ray field for the application of calibration and standardization.

5.1.1 Half-Value Layer Measurement (HVL)

Half-value layer (HVL) is measured by using electrometer and an ionization chamber. Ionization chamber was positioned at a distance of 100 cm along with central axis of the beam. Half-value layer i.e., the first and second HVL measurement was performed for different tube voltage (kV) with tube current (mA) by using additional Cu filter. For beam quality N-40, N-60, N-80, N-100, N-120, N-150 and N-200, we calculated half-value layer by using combination of ionization chamber and electrometer. For a specific beam quality, we added additional Cu filter of different thickness. We took three reading of electrometer for specific thickness. First reading is without any filter. The data obtained from the electrometer for 60 seconds. The electrometer must need pressure and temperature correction Then the data is plotted in the graph by using Microsoft Excel. In the vertical axis charge is selected in nC/min unit and in the X axis thickness is selected. By data interpolation, the first half-value layer and second are measured.

Table 5.1: Measurement of half-value layer (HVL) for tube potential 40 kV

Beam Quality	Tube potential	Tube current	Added Cu filter thickness in mm.	Electrometer reading (nC/min)	Half Value Layer in mm Cu	
					First	Second
N40	40 kV	10 mA	Without filter	12.54±0.002	0.097	0.198
			0.10	6.09±0.003		
			0.20	3.09±0.000		
			0.35	1.03±0.001		
			0.45	0.57±0.001		
			0.55	0.33±0.003		

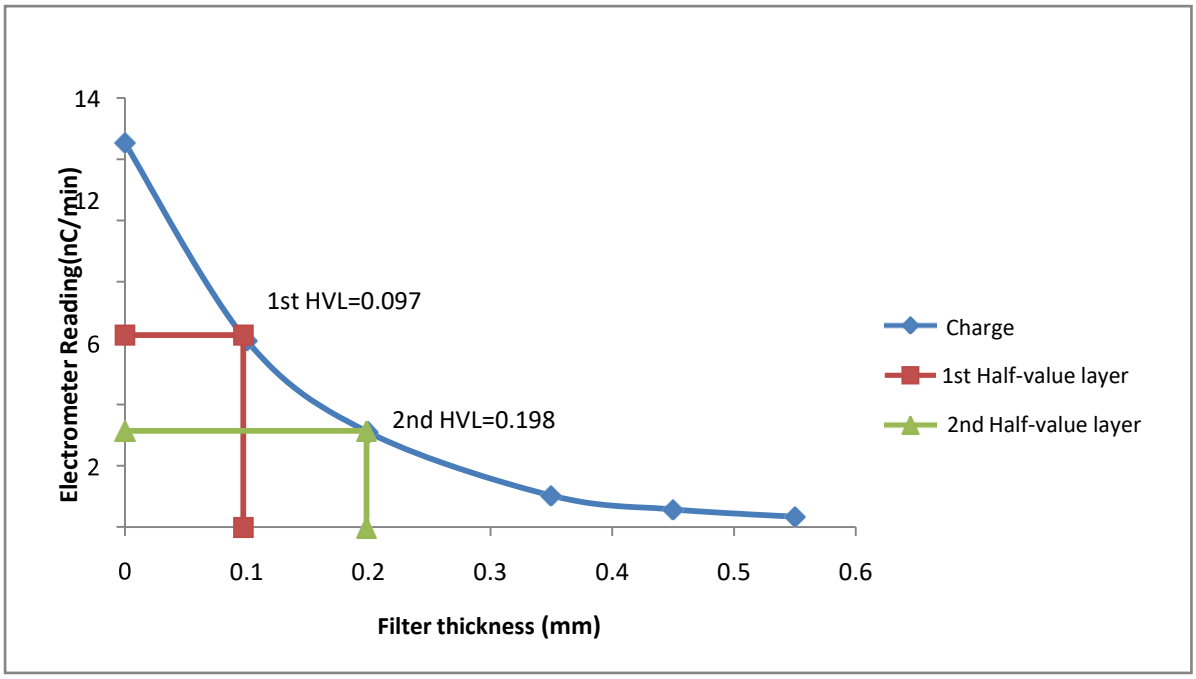

Fig. 5.1: Filter thickness Vs. electrometer reading for 40 kV tube potential.

From Fig. 5.1, we have found 1st HVL (half-value layer) 0.097 and 2nd HVL (half-value layer) 0.198 for tube potential 40 kV.

Table 5.2: Measurement of half-value layer (HVL) for tube potential 60 kV

Beam Quality	Tube potential	Tube current	Added Cu filter thickness in mm.	Electrometer reading (nC/min)	Half Value Layer in mm Cu	
					First	Second
N60	60 kV	10 mA	Without filter	27.03±0.001	0.252	0.538
			0.10	20.65±0.002		
			0.20	15.98±0.001		
			0.35	10.35±0.003		
			0.45	8.20±0.002		
			0.55	6.57±0.000		
			0.60	5.65±0.002		

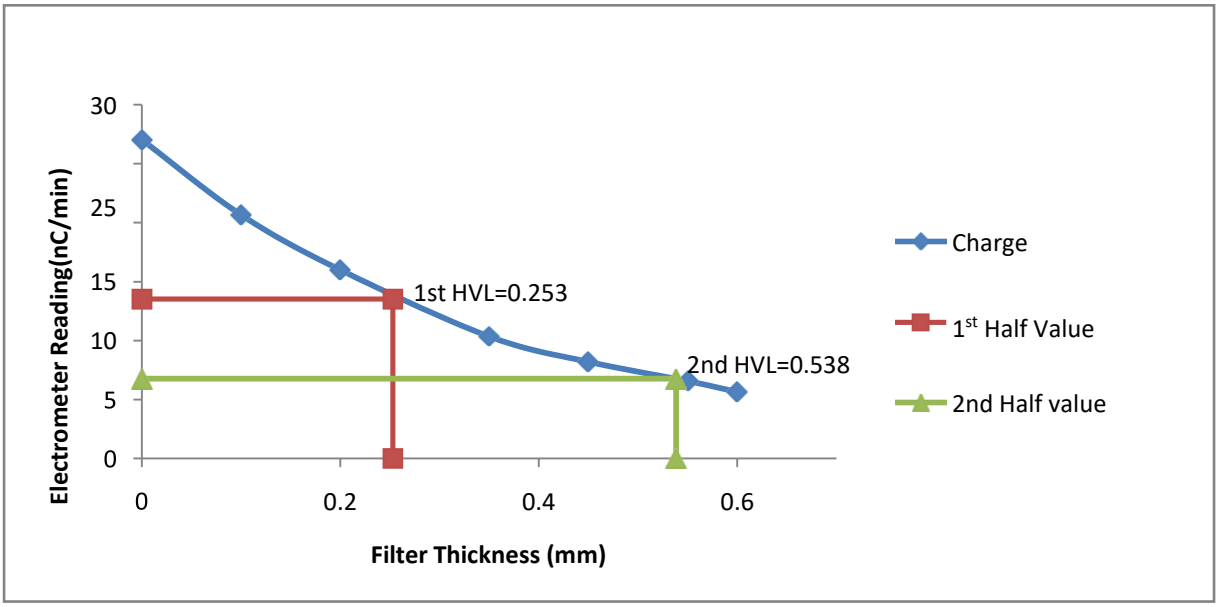

Fig. 5.2: **F**ilter thickness Vs electrometer reading for 60 kV tube potential.

From Fig. 5.2, we have found 1st HVL (half-value layer) 0.253 and 2nd HVL (half-value layer) 0.538 for tube potential 60 kV.

Table 5.3: Measurement of half-value layer (HVL) for tube potential 80 kV

Beam Quality	Tube potential	Tube current	Added Cu filter thickness in mm.	Electrometer reading (nC/min)	Half Value Layer in mm Cu	
					First	Second
N80	80 kV	10 mA	without filter	12.98±0.006	0.625	1.286
			0.35	8.79±0.004		
			0.55	7.19±0.002		
			0.70	5.78±0.004		
			0.90	4.78±0.000		
			1.05	4.03±0.002		
			1.25	3.36±0.003		
			1.40	2.87±0.002		

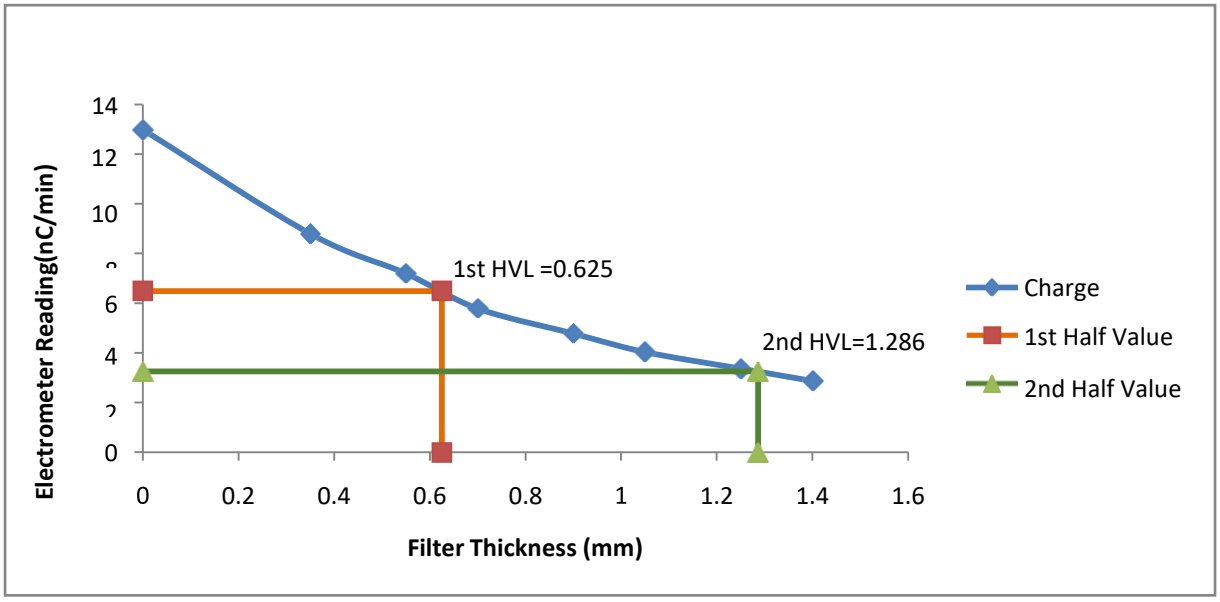

Fig. 5.3: Filter thickness Vs electrometer reading for 80 kV tube potential.

From Fig. 5.3, we have found 1st HVL (half-value layer) 0.625 and 2nd HVL (half-value layer) 1.286 for tube potential 80 kV.

Table 5.4: Measurement of half-value layer (HVL) for tube potential 100 kV

Beam Quality	Tube potential	Tube current	Added Cu filter thickness in mm.	Electrometer reading (nC/min)	Half Value Layer in mm Cu	
					First	Second
N100	100 kV	10 mA	without filter	6.81±0.002	1.074	2.333
			0.35	5.54±0.012		
			0.70	4.44±0.001		
			1.05	3.45±0.002		
			1.25	3.10±0.001		
			1.50	2.65±0.002		
			2.10	1.93±0.001		
			2.55	1.49±0.001		

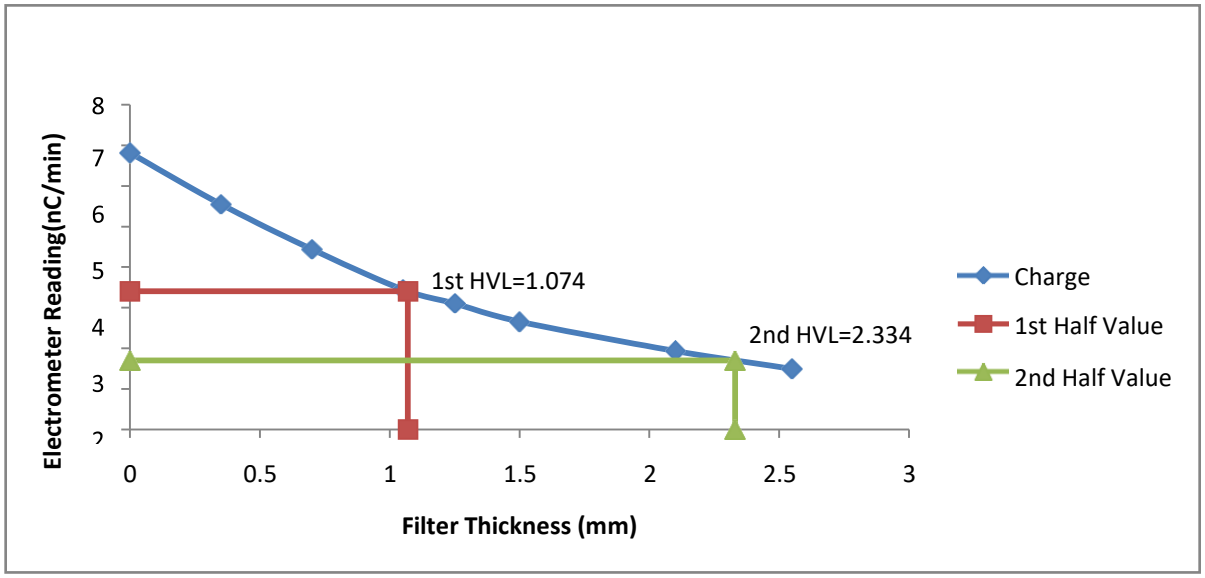

Fig. 5.4: Filter thickness Vs electrometer reading for 100 kV tube potential.

From Fig. 5.4, we have found 1st HVL (half-value layer) 1.074 and 2nd HVL (half-value layer) 2.334 for tube potential 100 kV.

Table 5.5: Measurement of half-value layer (HVL) for tube potential 120 kV

Beam Quality	Tube potential	Tube current	Added Cu filter thickness in mm.	Electrometer reading (nC/min)	Half Value Layer in mm Cu	
					First	Second
N120	120 kV	10 mA	without filter	7.25±0.005	1.844	3.774
			0.45	6.13±0.002		
			1.05	4.82±0.001		
			1.40	4.27±0.005		
			1.85	3.62±0.002		
			2.20	3.14±0.005		
			2.80	2.57±0.001		
			3.35	2.11±0.001		
			3.70	1.8±0.001		
			4.15	1.60±0.002		

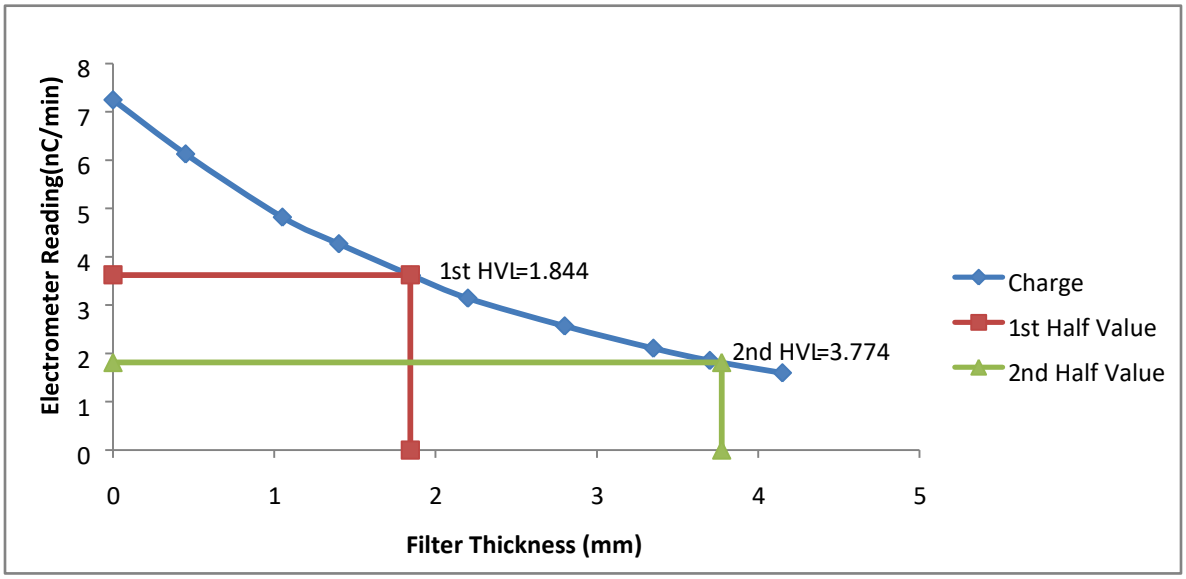

Fig. 5.5: Filter thickness Vs electrometer reading for 120 kV tube potential.

From Fig. 5.5, we have found 1st HVL (half-value layer) 1.844 and 2nd HVL (half-value layer) 3.774 for tube potential 120 kV.

Table 5.6: Measurement of half-value layer (HVL) for tube potential 150 kV

Beam Quality	Tube potential	Tube current	Added Cu filter thickness in mm.	Electrometer reading (nC/min)	Half Value Layer in mm Cu	
					First	Second
N150	150 kV	10 mA	without filter	53.01±0.002	2.572	5.257
			0.70	43.33±0.001		
			1.30	37.06±0.013		
			2.10	29.85±0.011		
			2.45	27.30±0.003		
			3.20	22.41±0.001		
			4.30	16.81±0.014		
			5.10	13.75±0.003		
			5.45	12.64±0.002		

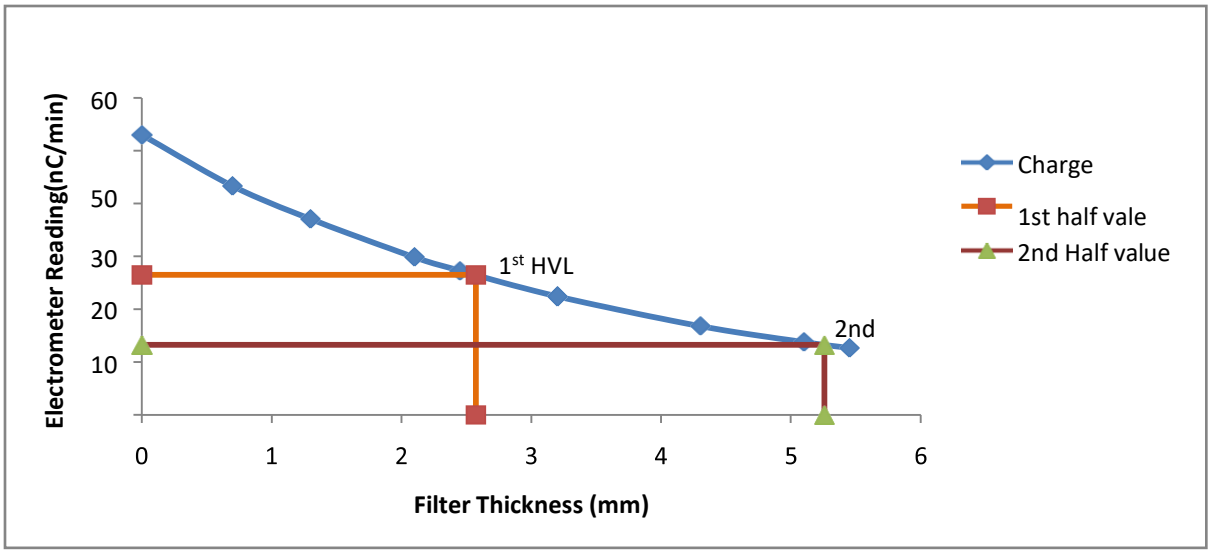

Fig. 5.6: Filter Thickness Vs electrometer reading for 150 kV tube potential.

From Fig. 5.6, we have found 1st HVL (half-value layer) 2.572 and 2nd HVL (half-value layer) 5.257 for tube potential 150 kV.

Table 5.7: Measurement of half-value layer (HVL) for tube potential 200 kV

Beam Quality	Tube potential	Tube current	Added Cu filter thickness in mm.	Electrometer reading (nC/min)	Half Value Layer in mm Cu	
					First	Second
N200	200 kV	10 mA	without filter	20.45±0.001	4.395	8.894
			1.05	17.19±0.003		
			2.10	14.68±0.002		
			3.20	12.30±0.001		
			4.30	10.36±0.003		
			5.30	8.95±0.011		
			6.15	7.74±0.010		
			7.45	6.41±0.001		
			9.00	5.02±0.002		
			10.00	4.24±0.002		

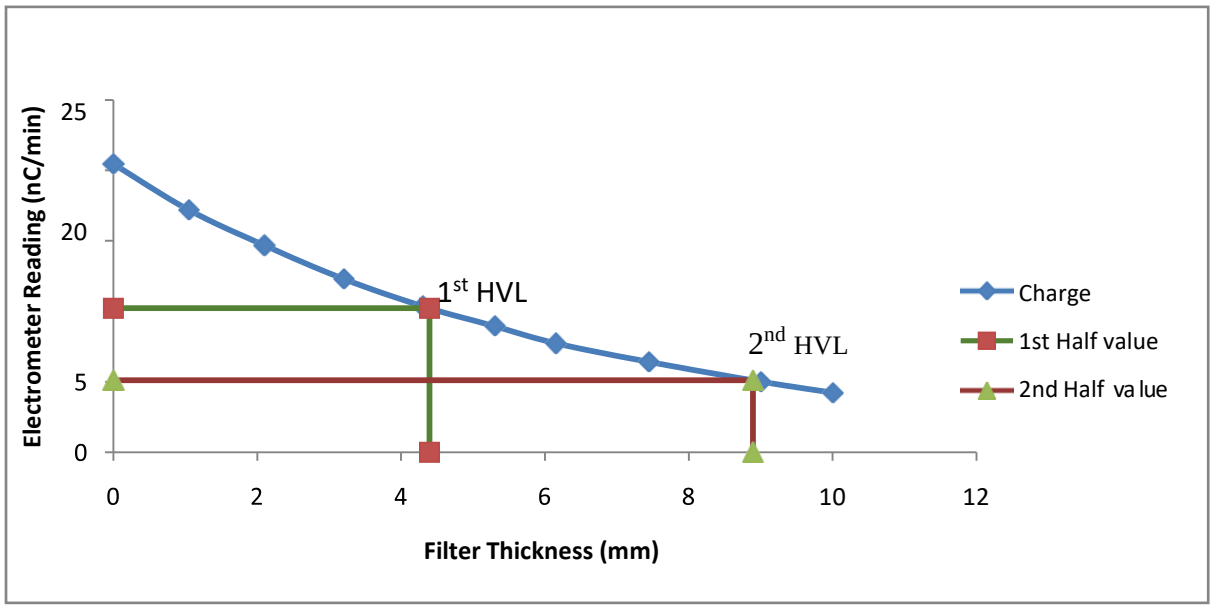

Fig. 5.7: Filter Thickness Vs electrometer reading for 200 kV tube potential.

From Fig. 5.7, we have found 1st HVL (half-value layer) 4.395 and 2nd HVL (half-value layer) 8.894 for tube potential 200 kV.

Table 5.8: Measurement of First and Second HVL for different kV

Measured 1st HVL and ISO 1st HVL are compared. Besides measured 2nd HVL and ISO 2nd HVL are also compared. They are given below:

Beam Quality	Observed 1st HVL	ISO Value 1st HVL	% of Deviation	Observed 2nd HVL	ISO value 2nd HVL	% of Deviation	Homogeneity coefficient
N40	0.10	0.08	-15.48%	0.20	0.18	-13.14%	0.50
N60	0.25	0.24	-5.42%	0.54	0.50	-7.6%	0.46
N80	0.63	0.58	-7.76%	1.29	1.20	-7.17%	0.49
N100	1.07	1.11	3.24%	2.33	2.28	-2.37%	0.46
N120	1.84	1.71	-7.84%	3.77	3.48	-8.45%	0.49
N150	2.57	2.36	8.98%	5.26	4.83	-8.86%	0.49
N200	4.40	3.99	-10.15%	8.89	8.04	-10.62%	0.49

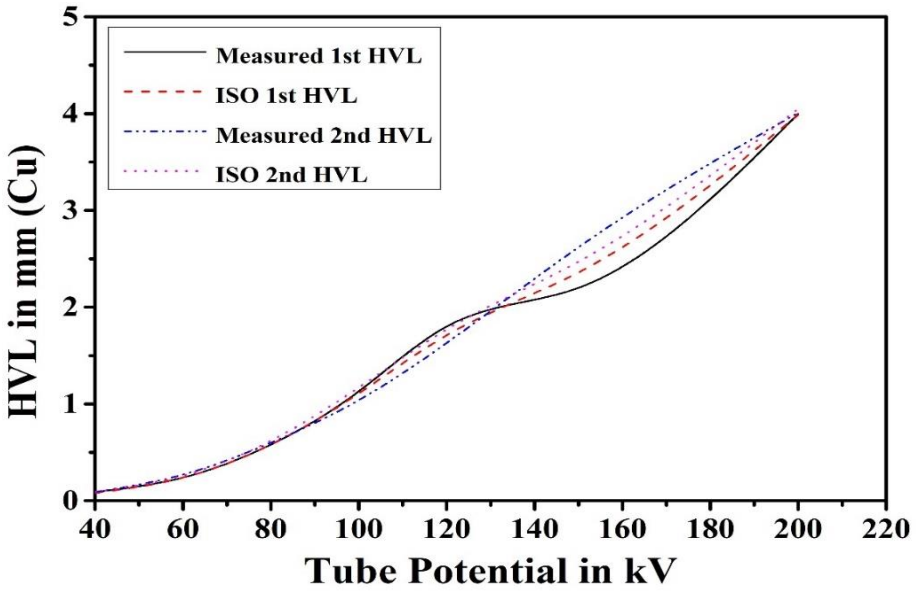

Fig.5.8: Comparison of observed and ISO 1st HVL and 2nd HVL in mm of Cu.

In figure 5.8, a comparison is shown between measured 1st HVL and ISO 1st HVL. Besides, measured 2nd HVL and ISO 2nd HVL are also compared.

5.1.2 Calculation of Homogeneity Coefficient

Homogeneity coefficients are obtained by dividing the 1st half-value layer with 2nd half-value layer. Homogeneity coefficients are measured for beam quality N40, N60, N80, N100, N120, N150, and N200. The measurement the of homogeneity coefficient is shown in Table 5.9 and also shown by Fig. 5.9.

Table 5.9: Homogeneity coefficient calculation data for Cu filter in mm

Beam Quality	Tube Potential (kV)	Current in mA	1st HVL of Cu	2nd HVL of Cu	Homogeneity Coefficient (h)
N40	40	10	0.10	0.20	0.50
N60	60		0.25	0.54	0.46
N80	80		0.63	1.29	0.49
N100	100		1.07	2.33	0.46
N120	120		1.84	3.77	0.49
N150	150		2.57	5.26	0.49
N200	200		4.40	8.89	0.49

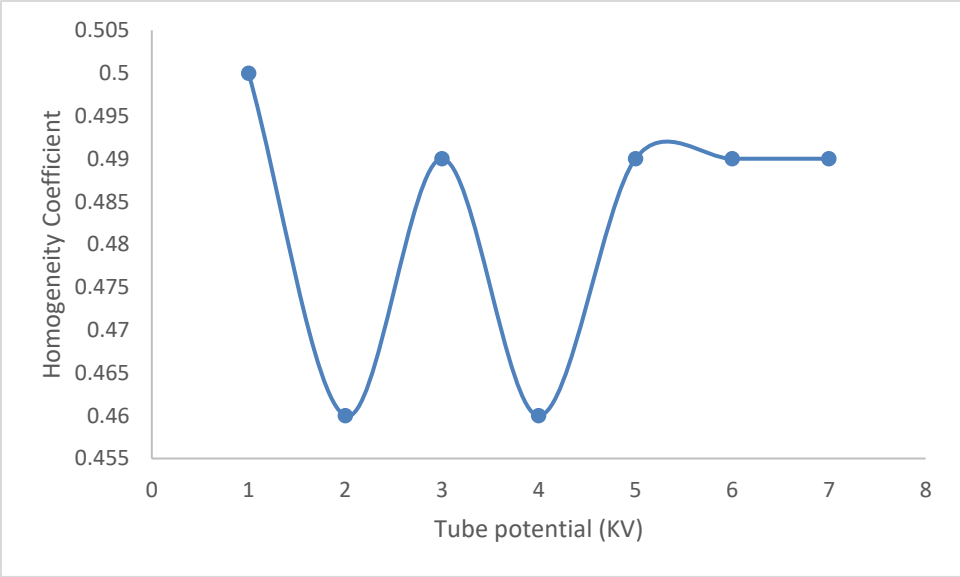

Fig.: 5.9: Homogeneity Coefficient for different tube potential.

In figure 5.9, homogeneity coefficient for different tube potentials are shown.

5.1.3: Measurement of Effective Energy and Quality Index

The effective energy (keV) was obtained from the interpolation value from Hubble mass attenuation coefficients. The effective energy for each beam was calculated by the half-value layer of this beam. The half-value layer (HVL) is important to calculate the effective energy of the beam. The quality index is the fraction of effective energy and tube potential.

Table 5.10: Calculation of Effective Energy and Quality Index

Tube Potential (kV)	Tube current (mA)	First HVL in mm of Cu	Effective energy in keV (measured)	Effective energy in keV (ISO value)	Percentag eof Deviation	Quality Index
40	10	0.10	33.35	33	-1.07	0.83
60		0.25	47.05	48	1.98	0.78
80		0.63	65.69	65	-1.06	0.82
100		1.07	81.38	83	1.95	0.81
120		1.84	103.73	100	-3.73	0.86
150		2.57	123.86	118	-4.96	0.83
200		4.40	178.61	164	-8.91	0.89

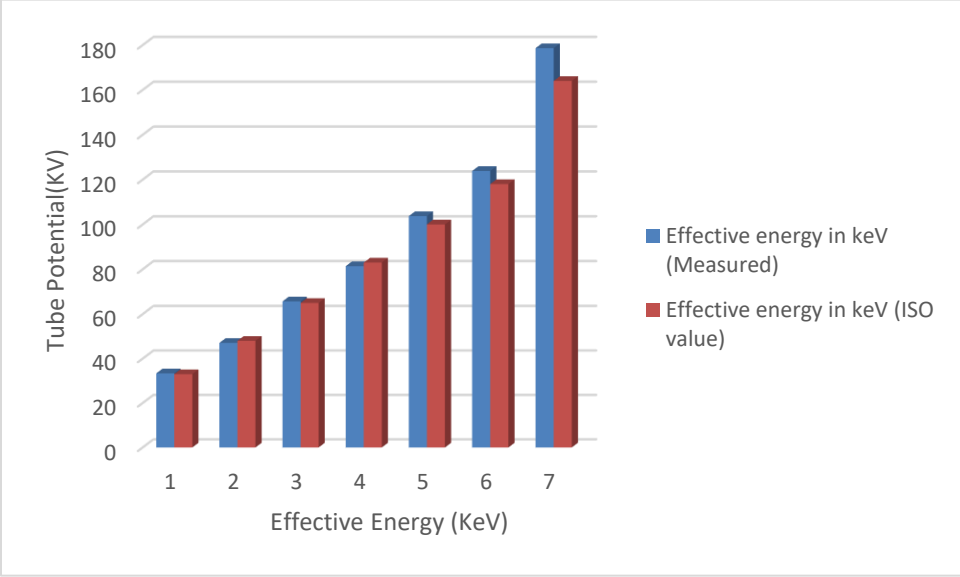

Fig. 5.10: Measured effective energy and ISO effective energy.

Calculated effective energies are shown in Table 5.10. In Fig. 5.10, Measured effective energy and ISO effective energy are shown by a bar graph.

5.2 Air kerma Rate Measurement at different distances

In this section, the air kerma rate is measured by using the base-1 electrometer and the ionization chamber reading. Kerma is actually the total kinetic energy of all charged particles generated by uncharged radiation per unit mass of some substance. The air kerma rate is measured for the X-ray beam irradiator. The electrometer value is recorded by changing the distance between the X-ray beam irradiator and the ionization chamber. The air kerma rate is calculated at 100 cm, 150 cm, 200 cm, 300 cm, and 400 cm.

From Table 5.11, describe the air kerma rate at different distances, which starts at 100 cm and finishes at 400 cm.

Table 5.11: Air kerma rate Calculation at SSD 100 cm with Buildup Cap

The air kerma rate is measured by using the base-1 electrometer and the ionization chamber. The electrometer value is recorded by changing the distance of 100 cm from the X-ray beam irradiator to the ionization chamber.

Beam Quality	Tube Potential (KV)	Tube Current (mA)	Average Electrometer Reading in (pC/min)	Pressure and Temperature (Ktp) factor	Chamber and Electrometer (NK) factor	Air Kerma Rate (mGy/h)
N40	40	10	12590.00	1.954	43.90	33.16
N60	60		25880.00	1.952	43.00	66.77
N80	80		13440.00	1.950	42.70	34.43
N100	100		6686.00	1.951	42.20	16.93
N120	120		7100.00	1.952	42.40	18.06
N150	150		54450.00	1.951	43.00	140.48
N200	200		20340.00	1.954	44.00	53.70

Table 5.12: Air kerma Rate Calculation at SSD 150 cm with buildup cap

The air kerma rate is measured by using the base-1 electrometer and the ionization chamber. The electrometer value is recorded by changing the distance of 150 cm from the X-ray beam irradiator to the ionization chamber.

Beam Quality	Tube Potential (KV)	Tube Current (mA)	Average Electrometer Reading in (pC/min)	Pressure and Temperature (Ktp) factor	Chamber and Electrometer (NK) factor	Air Kerma Rate (mGy/h)
N40	40	10	5197.00	1.012	43.90	13.85
N60	60		11330.00	1.012	43.00	29.58
N80	80		5832.00	1.951	42.70	14.94
N100	100		2883.00	1.951	42.20	7.30
N120	120		3184.00	1.951	42.40	8.10
N150	150		23660.00	1.012	43.00	61.04
N200	200		9131.00	1.012	44.00	24.11

Table 5.13: Air kerma Rate Calculation at SSD 200 cm with buildup cap

The air kerma rate is measured by using the base-1 electrometer and the ionization chamber. The electrometer value is recorded by changing the distance of 200 cm from the X-ray beam irradiator to the ionization chamber.

Beam Quality	Tube Potential (KV)	Tube Current (mA)	Average Electrometer Reading in (pC/min)	Pressure and Temperature (Ktp) factor	Chamber and Electrometer (NK) factor	Air Kerma Rate (mGy/h)
N40	40	10	3190.00	1.010	43.90	8.486
N60	60		6043.00	1.010	43.00	15.747
N80	80		3107.00	1.010	42.70	8.040
N100	100		1601.00	1.956	42.20	7.929
N120	120		1761.00	1.955	42.40	8.758
N150	150		12940.00	1.955	43.00	65.26
N200	200		5031.00	1.009	44.00	13.40

Table 5.14: Air kerma Rate Calculation at SSD 300 cm with buildup cap

The air kerma rate is measured by using the base-1 electrometer and the ionization chamber. The electrometer value is recorded by changing the distance of 300 cm from the X-ray beam irradiator to the ionization chamber.

Beam Quality	Tube Potential (KV)	Tube Current (mA)	Average Electrometer Reading in (pC/min)	Pressure and Temperature (Ktp) factor	Chamber and Electrometer (NK) factor	Air Kerma Rate (mGy/h)
N40	40	10	1326.00	1.954	43.90	6.825
N60	60		2682.00	1.954	43.00	13.521
N80	80		1301.00	1.954	42.70	6.513
N100	100		679.20	1.954	42.20	3.359
N120	120		728.10	1.954	42.40	3.619
N150	150		5743.00	1.954	43.00	28.952
N200	200		2151.00	1.956	44.00	11.107

Table 5.15: Air kerma Rate Calculation at SSD 400 cm with buildup cap

The air kerma rate is measured by using the base-1 electrometer and the ionization chamber. The electrometer value is recorded by changing the distance of 400 cm from the X-ray beam irradiator to the ionization chamber.

Beam Quality	Tube Potential (KV)	Tube Current (mA)	Average Electrometer Reading in (pC/min)	Pressure and Temperature (Ktp) factor	Chamber and Electrometer (NK) factor	Air Kerma Rate (mGy/h)
N40	40	10	712.4	1.952	43.90	3.660
N60	60		1450.00	1.949	43.00	7.291
N80	80		713.30	1.949	42.70	3.585
N100	100		378.40	1.949	42.20	1.865
N120	120		405.70	1.949	42.40	2.008
N150	150		3197.00	1.954	43.00	16.117
N200	200		1232.00	1.952	44.00	6.348

5.3 Calculation of Conversion coefficient of ambient dose equivalent

The calculation of the conversion coefficient of ambient dose equivalent is shown in Table 5.16. This coefficient is used to measure various dose equivalents, like personal dose equivalents and ambient dose equivalents.

Table 5.16: Measurement of Conversion Coefficient

Beam Quality	Mean Energy in keV	Effective Energy in keV	Measured H*(10)/Ka in SvGy-1	ISO H*(10)/Ka in SvGy-1	Percentage of deviation
N40	33	32.47	1.204736811	1.18	-2.19%
N60	48	46.16	1.606089948	1.59	-1.01%
N80	65	63.85	1.747142682	1.73	-0.98%
N100	83	83.13	1.709696337	1.71	0.018
N120	100	102.52	1.635754457	1.64	0.00
N150	118	113.57	1.595574807	1.58	-0.98
N200	164	165.97	1.456501429	1.46	0.00

Table 5.16 shows the ISO conversion coefficient and the measured conversion coefficient. The difference between the ISO conversion coefficient and the measured conversion coefficient is also shown in Table 5.16.

5.4 Ambient dose equivalent H*(10) measurement

The ambient dose equivalent at a point in radiation, is the dose equivalent that would be produced by the corresponding expanded and aligned field in the ICRU sphere at depth d, on the radius opposing the direction of the field. We measured the value of H*(10) by multiplying the conversion coefficient and air kerma rate, which were described before. In table 5.17, the measurement of the ambient dose is shown.

Table 5.17: Measurement of H*(10) for X-ray

Voltage (Kv)	Measured H*(10)/Ka in SvGy-1	Air Kerma Rate (mGy/h)	Measured H*(10)/Ka in µSvGy-1/hr
40	1.17	33.78	39522.60
60	1.56	65.07	101509.20
80	1.72	31.48	54145.60
100	1.703	16.07	27367.21
120	1.61	17.31	27869.10
150	1.57	12.95	20331.5
200	1.458	50.86	74153.88

5.5 Calculation of Personal Dose Equivalent $H_P(10)$ and $H_P(0.07)$

The ICRU and ICRP recommended the operational quantities Hp(10) and Hp(0.07) as the quantities to be determined for personal dose equivalent evaluations for highly penetrating and weakly penetrating radiations. These quantities are not measurable, hence to need to measure them on a suitable phantom, which is very sensitive for effective dose measurement by radiation workers.

A set of conversion coefficients of Hp (10) and Hp (0.07) for the ISO narrow beam series is derived from the fitting values and is presented in Table 5.18.

Table 5.18: Conversion coefficient for personal dose equivalent $H_P(10)$ and $H_P(0.07)$

Beam Quality	Effective Energy in KeV	Conversion Coefficient $H_P(10)$ (Sv/Gy)			Conversion Coefficient $H_P(0.07)$ (Sv/Gy)		
		ICRU Tissue Slab	PMMA Slab	ISO water Slab phantom	ICRU Tissue Slab	PMMA Slab	ISO water Slab phantom
N40	32.63	1.340	1.541	1.298	1.261	1.161	1.253
N60	44.73	1.631	1.504	1.657	1.5311	1.4073	1.5570
N80	64.84	1.885	1.7925	1.9315	1.723	1.6084	1.7655
N100	85.57	1.877	1.8239	1.9117	1.718	1.6694	1.7289
N120	102.52	1.805	1.7651	1.8473	1.665	1.6282	1.7040
N150	116.33	1.740	1.7085	1.7820	1.617	1.5877	1.6460

5.6 X-ray machine photon spectra simulation

The X-ray spectrum that satisfied the quality of the ISO narrow spectrum series N80-N200 generated from Model X80-225KV, Hopewell Design, Inc., USA, installed at the Secondary Standard Dosimetry Laboratory, Bangladesh Atomic Energy Commission, is therefore simulated with the Monte Carlo N Particle Transport Code. This code is a powerful geometry package that uses complex geometry to describe unions, intersections, and complements of cells that can be defined by the user's plan. A photon's history terminates when it reaches an energy of 1 keV. The energy loss of electrons for X-ray production by collision can be expressed by the Bethe-Bloch formula. In the present study, MCNP is run with default parameters that count for the photoelectric effect, the Compton effect, and pair production, including Fluorescence. The Thomson effect is accounted for by the modification of the cross section, and the Compton cross section is modified by the incoherent scattering cross section that corrects the electron binding effects.

X-ray spectra have been generated by the experimental condition satisfied with ISO radiation quality, which was determined by the attenuation analysis method, which gave spectra in terms of photon fluence and exposure. The simulated geometry (2-D view and 3-D view) of the X-ray machine is shown in Fig. 5.12.

Target: It is disk-shaped, angled at 20 degrees with respect to the incident electron beam direction. The thickness and radius of the target are 0.8 mm and 3 cm, respectively.

Exit Window: It is also disk-shaped with a thickness of 1mm, positioned 5 cm from the focal spot of the target.

Primary Collimator: It is designed by combining two truncated right-angle cones. It is 6.1 cm from the focal spot of the target. The radii of the first cone are 1.19 cm and 1.62 cm, whereas the radii of the second TRC (truncated right-angle cone) are 1.97 cm and 3.07 cm, respectively. The height of the collimator is 0.95 cm**.**

Secondary Collimator: It is composed of the combination of a right circular cylinder (RCC) and a truncated right-angle cone (TRC). It is 8.5 cm from the focal spot of the target, and its height is 1.91 cm.

Inherent Filter Assembly: Inherent filter assembly is associated with ISO narrow X-ray beam qualities. For 100 kVp, the filter assembly consists of a 2.5 mm Cu and 3.5 mm fixed

Al filter to cut off low-energy photons. Filter assembly is also different for different kVps. Inherent filter assembly is not the same for different kVp.

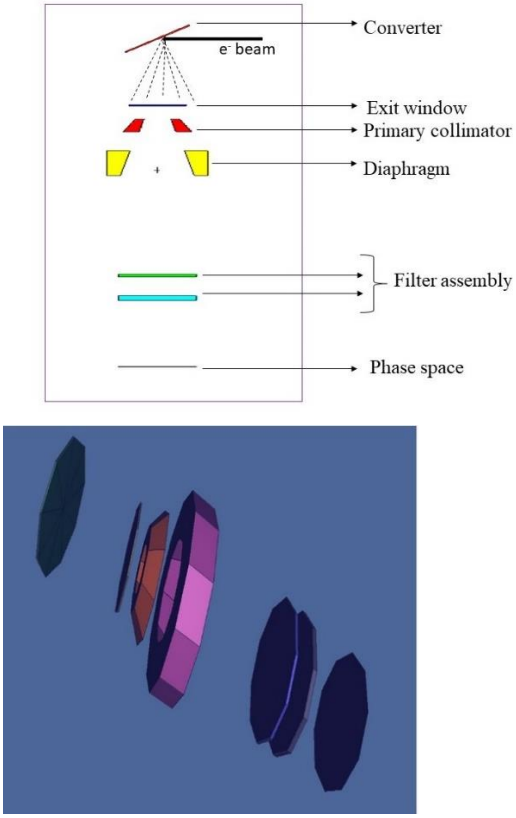

Fig. 5.12: Simulated geometry (2-D view and 3D view) of an X-ray machine.

In Fig. 5.12, a 2-D view of X-ray machine and a 3D view of the X-ray machine are simulated by creating a input file and declaring the necessary dimensions.

Creating an input file by declaring the necessary dimensions and source particle, X-ray machine input file is executed using the run mode of Visual Editor Windows for MCNP code. Then, we plotted X-ray photon spectra for 80 kV, 100 kV, 120 kV, 150 kV, and 200 kV. The calculated spectrum was generated from the experimental condition by the MCNP code.

5.7 Simulation of Back Scattering Factor

These spectral values were used in the present Monte Carlo calculations of back scatter factors for ISO water phantom of 30 cm × 30 cm × 30 cm and ICRU slab phantom of 30 cm × 15 cm × 30 cm. The MCNP-generated Back Scattering Factor (BSF) for ICRU slab phantom and ISO water phantom from the present study is summarized with experimental values and is given in Table 5.19 and Table 5.20.

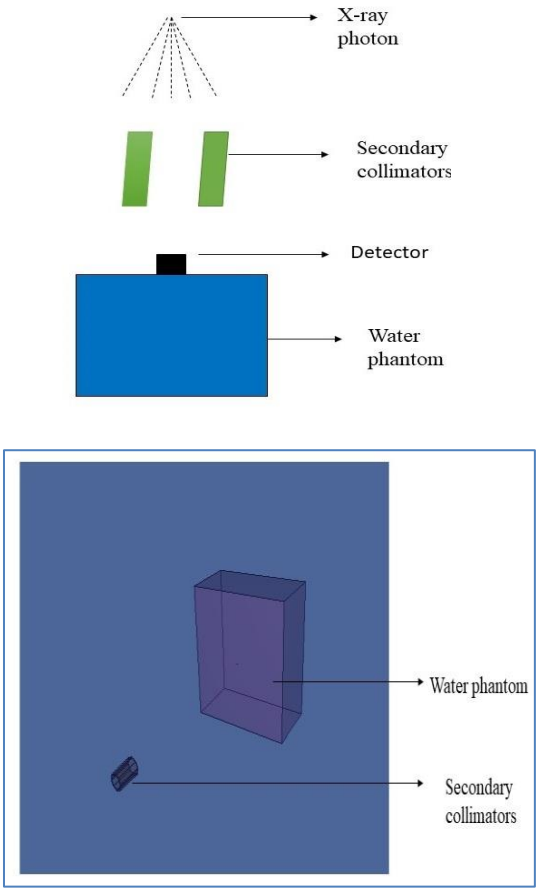

Fig. 5.13: Backscattering Factor (2-D view and 3-D view)

Using the spectra of X-ray beams as input, we performed simulation with the Montae Carlo Code (MCNP), in which the backscatter factor was calculated as the ratio of the water kerma at a point on the beam axis at the surface of a water phantom to the water kerma at the same point in the absence of the phantom. We considered a point source irradiating a water phantom of 30 cm × 30 cm × 30 cm, with a source-to-surface distance of 100 cm.

Table 5.19: MCNP calculated BSF values with observed values for ISO water phantom

Tube Potential (kV)	Backscattering factor (BSF)	
	MCNP Generated BSF calculated in the present study	Experimental Data
80	1.3665	1.3701
100	1.2974	1.2985
120	1.2536	1.2630
140	1.2060	1.2103

Using the spectra of X-ray beams as input, we performed simulation with the Montae Carlo Code (MCNP), in which the backscatter factor was calculated as the ratio of the water kerma at a point on the beam axis at the surface of an ICRU Slab phantom to the water kerma at the same point in the absence of the phantom. We considered a point source irradiating an ICRU Slab phantom of 30 cm × 15 cm × 30 cm with a source-to-surface distance of 100 cm.

Table 5.20: MCNP calculated BSF values with observed values for ICRU Slab phantom

Tube potential (KV)	Backscattering factor	
	MCNP Generated BSF calculated in the present study	Experimental Data
80	1.3698	1.3700
100	1.2975	1.2999
120	1.2543	1.2600
140	1.2027	1.2108

CHAPTER 6
CONCLUSION AND RECOMMENDATIONS

6.1 Conclusion

The use of X-ray facilities in calibrating radiation measuring equipment requires exact knowledge of the radiation field. In order to characterize the X-ray field, the half-value layer (HVL) is the first parameter to be found. From Tables 5.1 to 5.7, the first and second half-value thicknesses, respectively, for 40, 60, 80, 100, 120, 150, and 200 KV were measured from the graphs shown in Figs. 5.1 to 5.7. The measured values were compared with the ISO values, and the percentage of deviation and homogeneity coefficient were calculated as shown in Table 5.8. It is found that in the case of beam quality, N40 and N200 values are mostly deviated.
The air kerma rate is an important factor for analyzing the beam quality of an X-ray beam irradiator. It is calculated for different distances, like 100 cm, 150 cm, 200 cm, 300 cm, and 400 cm.

The effective energy (keV) is calculated by an established empirical relation, which is obtained by the interpolation value from the Hubble mass attenuation coefficient and compared with the ISO values. Except for beam quality N200, allother values were found within the range.

A set of conversion coefficients *(Sv/Gy)* for ambient dose equivalent H*(10) have been calculated for the ISO narrow beam spectrum series. The conversion coefficient for ambient dose equivalent H*(10) is calculated for monoenergetic photons. The derived values of conversion coefficients also showed good agreement with ISO values. The personnel dose equivalents Hp (10) and Hp (0.07) has also been calculated for various phantoms like the ICRU Tissue Slab, PMMA Slab, and ISO Water Slab phantom as a function of photon energy.

The Monte Carlo particle transport algorithm model is reputedly known as the actual physics of energy deposition by radiation in tissues. MCNP theoretical simulation is recognized as the most accurate dose calculation methods for complex patient geometry and tissue heterogeneity. X-ray photon spectra are generated by using the MCNP code for beam qualities N80, N100, N120, and N140. These MCNP-generated photon spectra were

used for the Monte Carlo of the backscattering factor (BSF). MCNP-generated back scattering factors (BSF) were calculated for beam qualities N80, N100, N120, and N140. At last, MCNP-generated back scattering factors (BSF) and experimental back scattering factors (BSF) were compared.

This study could be used to optimize the radiation protection system in Bangladesh and can be used by other researchers for further study of radiation protection and measurement.

6.2 Recommendations

Bangladesh is a country of around 160 million people. This 8th most populous country in the world has 13 to 15 lakh cancer patients, with about 2 lakh patients newly diagnosed with cancer each year. The Monte Carlo particle transport algorithm model is reputedly known as the actual physics of energy deposition by radiation in tissues. MCNP theoretical simulation is recognized as the most accurate dose calculation method for complex patient geometry and tissue heterogeneity, which is being planned for subsequent research activity.

- In the future study, our developed input files can be used in MCNP code for further study of the radiation protection system.
- In this research work, we calculated the back scatter for an X-ray irradiator, but in the future, using these developed input files, with necessary corrections, it will be possible to simulate a linear accelerator.

REFERENCES

ICRU (2016). ICRU Report Committee 26 on Operational Radiation Protection Quantities for External Radiation Operational Quantities and New Approach by ICRU Ann ICRP, 45, pp. 178-187.

ICRU and ICRP (2017). Final Draft for Consultation on Operational Quantities for External Radiation Exposure, Journal of ICRU, Oxford University press.

Otto, T., Hertel, N. E. (2018). The ICRU Proposal for New Operational Quantities for External Radiation, Radiat. Prot. Dosimetry, pp. 10-16.

Thompson, I. (1989). Calibration of Protection-Level Instruments, Conversion Coefficients (Sv/Gy) for the ISO Reference Photon Radiations, Journal of Radiation Protection, vol. 9, no. 3, pp. 203-205.

ISO (2019). Radiation protection: X and gamma reference radiation for calibrating dose meters and dose rate meters for determining their response as a function of photon energy, Part 1, International Organization of Standardization 4037-1, Geneva.

ICRP (1996). Conversion Coefficients for Use in Radiological Protection Against External Radiation. ICRP Publication 74, Annals of the ICRP, 26.

Iles, W.J. (1987). Conversion Coefficients from Air kerma to Ambient Dose Equivalent for the International Standards Organizations Wide, Narrow, and Low Series of Reference Filtered X-Radiation," NRPB-R206.

ICRP (1996). Conversion Coefficients for use in Radiological Protection against External Radiation, ICRP Publication 74, Ann. ICRP 26, 3/4, Oxford, Pergamon.

ISO (2019). Radiation protection: X and gamma reference radiation for calibrating dose meters and dose rate meters for determining their response as a function of photon energy, Part-1," International Organization of Standardization 4037-1, Geneva.

ICRP (2010). Conversion coefficients for radiological protection quantities for external radiation exposures", ICRP Publication 116, Ann. ICRP vol. 40, pp. 1–257.

Shier, D., Butler, J., and Lewis, R. (2009). Hole's Human Anatomy and Physiology**,** (twelfth ed.), McGraw-Hill, New York.

ISO (1999). X-ray and gamma reference radiations for calibrating dosimeters and dose rate meters and for determining their response as a function of photon energy, Part-3, International Organization of Standardization 4037-3, Geneva.

ICRP (1996). Conversion Coefficients for Use in Radiological Protection against External Radiation. ICRP Publication 74, Annals of the ICRP, 26.

Cember, H. and Jonson, T. E. (2009). Introduction to Health Physics", 4th edition, Northwestern University, Maxwell Macmillan International Editions, published by Pergamon Press.

Purohit, S., Kabir, S. M. E., and Rahman, M. S. (2017). A study of measurement of relative dose with various chamber for small field dosimetry of 6 MW photon, Journal of Nuclear science and Application, vol. 26, no.1 & 2, pp. 233-235.

Izumoto, Y., Fukutsu, K., and Takamura, K. (2020). Rapid detection of plutonium contamination with & without uranium contamination in wounds by X-ray fluorescence, Journal of Radiological Protection, vol. 40, no. 3, pp. 236-237.

Robin, H., Brendan, H. (2014). Advances in kilovoltage x-ray beam dosimetry, Phys. Med. Biol. 59, pp. 183-231.

Jung-Ha, K., Robin, H. (2010). An investigation of backscatter factors for kilo voltage X-rays: A comparison between Monte Carlo simulations and Gafchromic EBT film measurements", Phy. Medi. Biol. 55(3), pp. 783-97.

WHO (1982). Quality Assurance in Diagnostic Radiology, WHO, Geneva.

IAEA (2004). Optimization of the radiological protection of patients undergoing radiography, fluoroscopy, and computed tomography; final report of a coordinated research project in Africa, Asia, and eastern Europe, IAEA- TECDOC-1423.

Moschler, W.W. (1998). Calibration procedure for a direct scanning densitometer using gamma radiation", Wood and Fiber science, 20(3), pp. 297-303.

Desrosiers, M., DeWerd, L., Deye, J. (2013). The Importance of Dosimetry Standardization in Radiobiology, Journal of Research of the National Institute of Standards and Technology, 118, pp. 403–418.

Hopmans, J., and Dane, J., (2019). Calibration of a Dual-Energy Gamma Radiation System for Multiple Point Measurements in a Soil, Water Resources Research- Water Resources. 22. 1109-1114.

Clarke, R. W., Lavender, A., and Thomson, I. M. G. (1967). Experience Gained in Operating a Dosimeter Calibration Facility, Health Physics.

Rahman, M. S. (2002). External and Internal Radiation Dosimetry for Workers: Maintenance and Calibration of Radiation Measuring Instruments", Final Technical Report, Nuclear Researcher Exchange Program, p. 23-64.

Khalid, R.O. (2005). Calibration of a Radiation Survey Meter Using a Cs-137 Gamma Source", University of Khartoum, Khartoum, Sudan.

Sumaiya, P. (2015). Dosimetry of the gamma field in characterizing radiation measuring instruments in Bangladesh, M.Sc. Thesis.

Masud., K. (2017). Dosimetry for measurement of ISO radiation quality and calibration protection level chambers", BSc. Thesis.

Bartlett, D. T., Dimbylow, P. J., and Francis, T. M. (1986). Calculations of the Energy and Angle Dependence of Response of a Simplified Design of Photon Personal Dosimeter and its Relationship with the Recommended ICRU Calibration Quantity, Radiation Protection Dosimetry.

Siddiqua, T., and Rahman, M. S., (2021). Determination of calibration X-ray beam qualities and establish a set of conversion coefficients for calibration of radiation protection in diagnostic radiology", East Eur. Journal of Physics, pp. 55-61.

Chan, H-P and Doi, K. (1981). Monte Carlo simulation studies of backscatter factors in mammography, Radiology 139, 195-199.

Seco, J., and Verhaegen, F. (2016). Monte Carlo Techniques in Radiation Therapy", 1st ed. CRC Press.

Oliveira, A. C. H., Vieira, J. W., Santana, M. G. and Lima, F. R. A. (2013). Monte Carlo Simulation of a Medical Linear Accelerator for Generation of Phase Spaces," p. 15.

Pelowitz, D. B. (2008). MCNPXTM USER'S MANUAL: Version 2.6.0. Los Alamos National Laboratory (LANL).

Pelowitz, D. B. (2008). MCNPX USER'S MANUAL: Los Alamos National Laboratory (LANL), p. 551.

Shultis, J. K. and Faw, R. E. (2011). AN MCNP PRIMER. Los Alamos National Laboratory (LANL).

ICRU (2016). ICRU Report Committee 26 on Operational Radiation Protection Quantities for External Radiation Operational Quantities and New Approach by ICRU Ann ICRP, 45, pp. 178-187.

ICRP (1996). Conversion Coefficients for Use in Radiological Protection Against External Radiation, ICRP Publication 74, Annals of the ICRP, 26.

Siddiqua, T., and M. S. Rahman, M. S. et al., (2021). Determination of calibration X-ray beam qualities and establish of a set of conversion coefficients for calibration of radiation protection in diagnostic radiology", East European Journal of Physics, pp. 55-61.

Leo, W. R. (1993). Techniques for Nuclear and Particle Physics Experiments, book, second edition, 37.

Publication

Nupur, R.P., Rahman, M.S., Rahman, A. Z. & Siddiqua, T. (2023). Characterization of X-ray reference beam to establish a set of conversion coefficients for the calibration of radiation measuring equipment and Calculation of BSF with MCNP code, American Journal of Biomedical Science & Research. ISSN: 2642-1747.